

Direct photons at forward rapidities in high-energy pp collisions

B. Z. Kopeliovich^{1,2}, E. Levin³, A. H. Rezaeian¹, and Ivan Schmidt¹

¹*Departamento de Física y Centro de Estudios Subatómicos,
Universidad Técnica Federico Santa María,
Casilla 110-V, Valparaíso, Chile*

²*Joint Institute for Nuclear Research, Dubna, Russia*

³*Department of Particle Physics,
School of Physics and Astronomy,
Raymond and Beverly Sackler Faculty of Exact Science,
Tel Aviv University, Tel Aviv, 69978, Israel*

We investigate direct photon production in pp collisions at the energies of RHIC, CDF and LHC, at different rapidities employing various color-dipole models. The cross section peaks at forward rapidities due to the abelian dynamics of photon radiation. This opens new opportunities for measurement of direct photons at forward rapidities, where the background from radiative hadronic decays is strongly suppressed. Our model calculations show that photon production is sensitive to the gluon saturation effects, and strongly depends on the value of the anomalous dimension.

PACS numbers: 13.85.QK, 13.60.Hb, 13.85.Lg

I. INTRODUCTION

Photons radiated in hadronic collisions not via hadronic decays are usually called direct. They carry important information about the collision dynamics, not disturbed by final state interactions. In particular, the hadronization stage is absent, so the theoretical interpretation is simpler than in the case of hadron production. A unified description for radiation of virtual (Drell-Yan reaction) and real photons within the color dipole approach was proposed in [1, 2]. This description does not need to be corrected either for higher order effects (K-factor, large primordial transverse momentum), or for the main higher twist terms¹. The corresponding phenomenology is based on the universal dipole cross section fitted to DIS data and provides a rather good description of data, both the absolute normalization and the transverse momentum dependence [4]. Predictions of the inclusive direct photon spectra for the LHC at midrapidity and the azimuthal asymmetry of produced prompt photons in the same framework are given in Refs. [5, 6]. Comparison with the predictions of other approaches at the LHC can be found in Refs. [7, 8].

Intensive study of the dynamics of hadronic interactions at high energies and search for signatures of nonlinear QCD effects, like saturation [9], or color glass condensate (CGC) [10], have led to considerable experimental progress towards reaching smallest Bjorken x . The typical experimental set up at modern colliders allows to detect particles produced in hard reactions in the central rapidity region, while the most energetic ones produced at forward (backward) rapidities escape detection. The first dedicated measurements of hadron production at forward rapidities, by the BRAHMS experiment in deuteron-gold collisions at RHIC [11], disclosed an interesting effect of nuclear suppression, which can be interpreted

as a breakdown of QCD factorization [12]. The zero degree calorimeters detecting neutral particles, neutrons and photons, at maximal rapidities are being employed at RHIC and are planned to be installed at LHC. One could increase the transverse momentum coverage of these detectors by moving them away from the beam axis. Through this note we would like to encourage the experimentalists to look up at these opportunities.

The important advantage of measurements of direct photons at forward rapidities is a significant enhancement of the signal-to-background ratio. Indeed, the photons radiated by the electric current of the projectile quarks, which stay in the fragmentation region of the beam, form a bump at forward rapidities (see Fig. 5). At the same time, gluons are radiated via nonabelian mechanisms by the color current which flows across the whole rapidity interval. Therefore gluons are radiated mainly in the central rapidity region [13], and are strongly suppressed in the beam fragmentation region. Such a suppression is even more pronounced for hadrons from gluon fragmentation, and for photons from radiative decays of those hadrons. Another source of background photons, hadrons produced via fragmentation of the valence quarks is also strongly suppressed due to the shift towards small fractional momenta related to the quark fragmentation function and the kinematics of radiative decay. Thus, direct photon production at forward rapidities should be substantially cleared up.

Here we perform calculations for direct photon production at large p_T and various rapidities in proton-proton collisions at the energies of RHIC, Tevatron and LHC. We employ the color dipole approach and compare the predictions of several contemporary models for the dipole cross section, based on the idea of gluon saturation.

¹ Some higher twist corrections, which are specific for forward rapidities, still have to be added [3].

II. PHOTON RADIATION IN THE COLOR DIPOLE FORMALISM

Production of direct photons in the target rest frame should be treated as electromagnetic bremsstrahlung by a quark interacting with the target. In the light-cone dipole approach the transverse momentum p_T distribution of photons radiated by a projectile quark interacting with a target nucleon, integrated over the final quark transverse momentum, can be written in impact parameter representation in the factorized form [2, 4],

$$\frac{d\sigma(qp \rightarrow \gamma X)}{d(\ln\alpha) d^2\vec{p}_T}(\vec{p}_T, \alpha) = \frac{1}{(2\pi)^2} \sum_{in,f} \int d^2r_1 d^2r_2 \times e^{i\vec{p}_T \cdot (\vec{r}_1 - \vec{r}_2)} \phi_{\gamma q}^*(\alpha, \vec{r}_1) \phi_{\gamma q}(\alpha, \vec{r}_2) \Sigma_\gamma(x_2, \vec{r}_1, \vec{r}_2, \alpha), \quad (1)$$

where \vec{r}_1 and \vec{r}_2 are the quark-photon transverse separations in the direct and complex conjugated amplitudes respectively; $\alpha = p_\gamma^+ / p_q^+$ denotes the fractional light-cone (LC) momentum of the radiated photon. Correspondingly, the transverse displacements of the recoil quarks in the two amplitudes are αr_1 and αr_2 respectively. The LC distribution amplitude for the $q\gamma$ Fock component with transverse separation \vec{r} has the form,

$$\phi_{\gamma q}(\alpha, \vec{r}_T) = \frac{\sqrt{\alpha_{em}}}{2\pi} \chi_f \hat{O} \chi_i K_0(m_q \alpha r_T). \quad (2)$$

Here $\chi_{i,f}$ are the spinors of the initial and final quarks and $K_0(x)$ is the modified Bessel function. The operator \hat{O} has the form,

$$\hat{O} = i m_f \alpha^2 \vec{e}^* \cdot (\vec{n} \times \vec{\sigma}) + \alpha \vec{e}^* \cdot (\vec{\sigma} \times \vec{V}) - i(2 - \alpha) \vec{e}^* \cdot \vec{V}, \quad (3)$$

where \vec{e} is the polarization vector of the photon; \vec{n} is a unit vector along the projectile momentum; and \vec{V} acts on \vec{r}_T . The effective quark mass m_q serves as infra-red cutoff parameter, which we fix at $m_q \approx 0.14$ GeV, since all dipole parametrizations considered in this paper also assume the light quark mass equal to 0.14 GeV.

In equation (1) the effective dipole cross-section Σ_γ is a linear combination of the $q\bar{q}$ dipole-proton cross sections,

$$\begin{aligned} \Sigma_\gamma(x_2, \vec{r}_1, \vec{r}_2, \alpha) &= \frac{1}{2} \{ \sigma_{q\bar{q}}(x_2, \alpha r_1) + \sigma_{q\bar{q}}(x_2, \alpha r_2) \} \\ &- \frac{1}{2} \sigma_{q\bar{q}}(x_2, \alpha(\vec{r}_1 - \vec{r}_2)). \end{aligned} \quad (4)$$

Here and in what follows $x_{1,2}$ are the Bjorken variable of the beam and target partons,

$$x_{1,2} = \frac{p_T}{\sqrt{s}} e^{\pm\eta}, \quad (5)$$

and η is the photon rapidity in the c.m. of pp collision.

Since only quarks and antiquarks can radiate photons, the hadronic cross section is given by the convolution of the partonic cross section Eq. (1) with the proton structure function

F_2^p [4, 14, 15],

$$\frac{d\sigma(pp \rightarrow \gamma X)}{dx_F d^2p_T} = \frac{1}{x_1 + x_2} \int_{x_1}^1 d\alpha F_2^p\left(\frac{x_1}{\alpha}, Q^2\right) \frac{d\sigma(qp \rightarrow \gamma X)}{d\alpha d^2p_T}, \quad (6)$$

where $x_F = x_1 - x_2$ is the Feynman variable. This relation needs commenting. The transverse momentum distribution of quark bremsstrahlung should be convoluted with the primordial transverse motion of the projectile quark. Differently from the parton model, in the dipole approach one should rely on the quark distribution function taken at a soft scale. Evolution to the hard scale is performed via gluon radiation, which is encoded into the phenomenological dipole cross section fitted to DIS data for the proton structure function. Since the quark primordial motion with a small (soft) mean transverse momentum does not affect the photons radiated with large p_T [4], we neglect the transverse momentum convolution and use the integrated quark distribution.

However, a word of caution is in order. The dipole cross section $\sigma_{q\bar{q}}(x_2, r)$ includes gluon radiation which performs the Q^2 evolution and leads to an increase of the transverse momentum of the projectile quark. However, it misses the Q^2 evolution of the x_1 -distribution, which is especially important at forward rapidities (see discussion in [16]), since the quark distribution falls off at $x_1 \rightarrow 1$ much steeper at high Q^2 . In order to account for this effect and provide the correct x_1 -distribution, we take the integrated quark distribution in (6) at the hard scale.

We use the parametrization for the proton structure function given in Ref. [17]. Following Ref. [4], for the hard scale entering the proton structure function in Eq. (6), we choose $Q = p_T$.

III. MODELS FOR THE DIPOLE CROSS SECTION

The dipole cross-section is theoretically unknown and should be fitted to data. Several parametrizations proposed in the literature are employed here to investigate the uncertainties and differences among various models.

A popular parametrization proposed by Golec-Biernat and Wüsthoff (GBW) model [18] is based on the idea of gluon saturation. This model is able to describe DIS data with the dipole cross-section parametrized as,

$$\sigma_{q\bar{q}}^{\text{GBW}}(x, \vec{r}) = \sigma_0 \left(1 - e^{-r^2 Q_s^2(x)/4} \right), \quad (7)$$

where x -dependence of the saturation scale is given by $Q_s^2(x) = (x_0/x)^\lambda \text{ GeV}^2$. The parameters $\sigma_0 = 20.1$ mb, $x_0 = 5.16 \times 10^{-4}$, and $\lambda = 0.289$ were determined from a fit to F_2 without charm quarks. A salient feature of the model is that for decreasing x , the dipole cross section saturates at smaller dipole sizes. The saturation scale in the GBW reduces with the inclusion of the charm quark [19]. After inclusion of the charm quark with mass $m_c = 1.5$ GeV, the parameters of the GBW model changed to $\sigma_0 = 23.9$ mb, $x_0 = 1.11 \times 10^{-4}$, and $\lambda = 0.287$. Both parametrization sets give a good description of DIS data at $x < 0.01$ and $Q^2 \in [0.25, 45]$ [19].

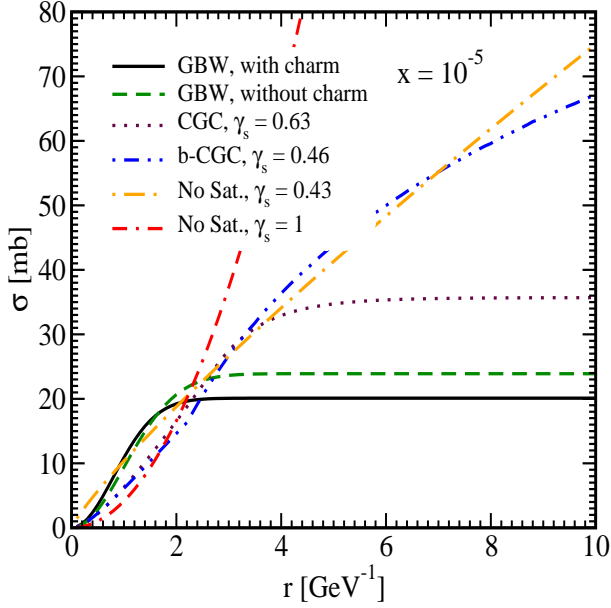


FIG. 1: The total dipole-proton cross section $\sigma_{q\bar{q}}(x, r)$ at a fixed $x = 10^{-5}$ in various dipole models introduced in Sec. III.

One of the obvious shortcomings of the GBW model is that it does not match the QCD evolution (DGLAP) at large values of Q^2 . This failure can be clearly seen in the energy dependence of $\sigma_{tot}^{q\bar{q}}$ for $Q^2 > 20 \text{ GeV}^2$, where the model predictions are below the data [18, 20].

A modification of the GBW dipole parametrization model, Eq. (7), was proposed in Ref. [20] by Bartels, Golec-Biernat and Kowalski (GBW-DGLAP)

$$\sigma_{q\bar{q}}^{\text{GBW-DGLAP}}(x, \vec{r}) = \sigma_0 \left(1 - \exp \left(- \frac{\pi^2 r^2 \alpha_s(\mu^2) x g(x, \mu^2)}{3 \sigma_0} \right) \right), \quad (8)$$

where the scale μ^2 is related to the dipole size by

$$\mu^2 = \frac{C}{r^2} + \mu_0^2. \quad (9)$$

Here the gluon density $g(x, \mu^2)$ is evolved to the scale μ^2 with the leading order (LO) DGLAP equation. Moreover, the quark contribution to the gluon density is neglected in the small x limit. The initial gluon density is taken at the scale $Q_0^2 = 1 \text{ GeV}^2$ in the form

$$xg(x, \mu^2) = A_g x^{-\lambda_g} (1-x)^{5.6}, \quad (10)$$

where the parameters $C = 0.26$, $\mu_0^2 = 0.52 \text{ GeV}^2$, $A_g = 1.20$ and $\lambda_g = 0.28$ are fixed from a fit to the DIS data for $x < 0.01$ and in a range of $Q^2 \in [0.1, 500] \text{ GeV}^2$ [20]. The dipole size determines the evolution scale μ^2 through Eq. (9). The evolution of the gluon density is performed numerically for every dipole size r during the integration of Eq. (1). Therefore, the DGLAP equation is now coupled to our master equation (1). It is important to stress that the GBW-DGLAP model preserves the successes of the GBW model at low Q^2 and its saturation

property for large dipole sizes, while incorporating evolution of the gluon density by modifying the small- r behaviour of the dipole size.

Since the linear DGLAP evolution may not be appropriate for the saturation regime, Iancu, Itakura and Munier proposed an alternative color glass condensate (CGC) model [21], based on the Balitsky-Kovchegov (BK) equation [22]. The dipole cross section is parametrized as,

$$\sigma_{q\bar{q}}^{\text{CGC}}(x, r) = \sigma_0 \begin{cases} \mathcal{N}_0 \left(\frac{r Q_s}{2} \right)^{2 \left(\gamma_s + \frac{1}{\kappa \lambda Y} \ln \frac{2}{r Q_s} \right)} & : r Q_s \leq 2 \\ 1 - e^{-A \ln^2(B r Q_s)} & : r Q_s > 2 \end{cases}, \quad (11)$$

where $Q_s \equiv Q_s(x) = (x_0/x)^{\lambda/2} \text{ GeV}$, $Y = \ln(1/x)$, and $\kappa = \chi''(\gamma_s)/\chi'(\gamma_s)$ where χ is the LO BFKL characteristic function. The coefficients A and B in the second line of (11) are determined uniquely from the condition that $\sigma(x, r)$, and its derivative with respect to $r Q_s$, are continuous at $r Q_s = 2$:

$$A = - \frac{\mathcal{N}_0^2 \gamma_s^2}{(1 - \mathcal{N}_0)^2 \ln(1 - \mathcal{N}_0)}, \quad B = \frac{1}{2} (1 - \mathcal{N}_0)^{-\frac{(1 - \mathcal{N}_0)}{\mathcal{N}_0 \gamma_s}}. \quad (12)$$

The parameters $\gamma_s = 0.63$ and $\kappa = 9.9$ are fixed at the LO BFKL values. The others parameters $\mathcal{N}_0 = 0.7$, $\sigma_0 = 35.7 \text{ mb}$, $x_0 = 2.7 \times 10^{-7}$ and $\lambda = 0.177$ were fitted to F_2 for $x < 0.01$ and $Q^2 < 45 \text{ GeV}^2$ and including a charm quark with $m_c = 1.4 \text{ GeV}$. Notice that for small $r Q_s \leq 2$, the effective anomalous dimension $1 - \gamma_s$ in the exponent in the upper line of Eq. (11) rises from the LO BFKL value towards the DGLAP value.

Notice that calculation of the p_T -distribution given by Eq. (1) needs only knowledge of the total dipole cross section and is independent of the impact parameter dependence of the partial elastic dipole-proton amplitude. Nevertheless, we consider also the model proposed by Watt and Kowalski [23]. Although the main focus of this model is the impact parameter dependence (b-CGC), which is irrelevant for our calculations, the integrated cross section is different from the above mentioned models,

$$\sigma_{q\bar{q}}^{\text{b-CGC}}(x, r) = 2 \int d^2 b \sigma_{q\bar{q}}^{\text{CGC}}(x, r, b), \quad (13)$$

where $\sigma_{q\bar{q}}^{\text{CGC}}(x, r, b)$ is given by Eq. (11) with the saturation scale Q_s which now depends on impact parameter,

$$Q_s \equiv Q_s(x, b) = \left(\frac{x_0}{x} \right)^{\frac{\lambda}{2}} \left[\exp \left(- \frac{b^2}{2 B_{\text{CGC}}} \right) \right]^{\frac{1}{2 \gamma_s}}. \quad (14)$$

The parameter $B_{\text{CGC}} = 7.5 \text{ GeV}^{-2}$ is fitted to the t -dependence of exclusive J/Ψ photoproduction. It has been shown that if one allows the parameter γ_s to vary along side with other parameters (in contrast with CGC fitting procedure where γ_s is fixed with LO BFKL value), it results in a significantly better description of data for F_2 with the value of $\gamma_s = 0.46$, which is remarkably close to the value of $\gamma_s = 0.44$ recently obtained from the BK equation [24]. Other parameters obtained from the fit are: $\mathcal{N}_0 = 0.558$, $x_0 = 1.84 \times 10^{-6}$ and $\lambda = 0.119$.

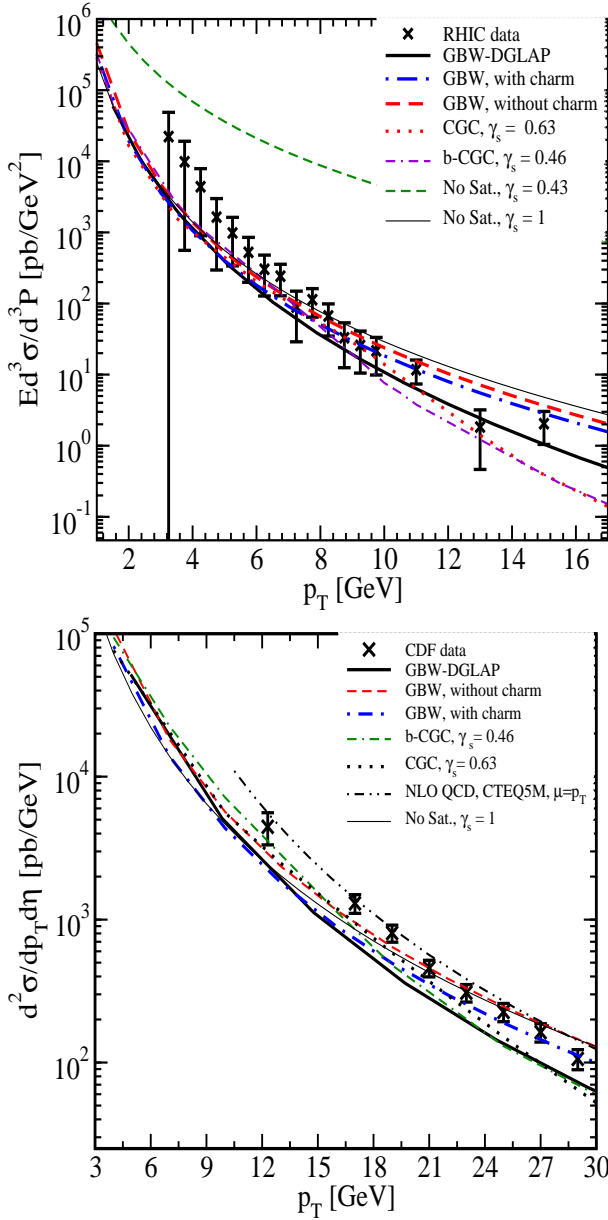


FIG. 2: Inclusive direct photon spectra calculated with various color-dipole models at mid-rapidity $\eta = 0$ at the energies of RHIC, $\sqrt{s} = 200$ GeV (upper panel), and Tevatron, $\sqrt{s} = 1.8$ TeV (lower panel). The NLO QCD curve is from the authors of reference [27] (given in table 3 of Ref. [28]). Experimental data are from the PHENIX experiment [29] at $\eta = 0$, and from the CDF experiment [28, 30] at $|\eta| < 0.9$. The error bars are the linear sum of the statistical and systematic uncertainties.

In order to demonstrate the importance of saturation, we will also use a non-saturated model (No Sat) fitted to F_2 with $x \leq 0.01$ and $Q^2 \in [0.25, 45]$ GeV²:

$$\frac{d\sigma_{q\bar{q}}^{\text{No Sat}}}{d^2\vec{b}} = 2\mathcal{N}_0 \left(\frac{rQ_s}{2} \right)^{2\gamma_s} \quad (15)$$

where Q_s is defined in Eq. (14) and the other parameters are given by $\gamma_s = 0.43$, $\mathcal{N}_0 = 0.568$, $x_0 = 1.34 \times 10^{-6}$ and

$\lambda = 0.109$ [23]. Surprisingly, the fit obtained with such an oversimplified model is as good as the other models with $\chi^2/\text{d.o.f.} = 0.92$ (although it should certainly fail to explain data on diffractive DIS [25], which are sensitive mainly to large size dipoles).

At first sight this result could be used as an argument that the data is not sensitive to the saturation effect. However, the actual meaning of this exercise is quite opposite. It is well known that the saturation effects start being essential when the anomalous dimension reaches the value $\gamma_{cr} = 1 - \gamma_s = 0.37$ (see Refs. [9, 26]). Therefore, what we actually demonstrate is that the value of the anomalous dimension should be larger than γ_{cr} , and because of this the saturation effects have to be taken into account. Summarizing, we can claim that direct photon production is sensitive to saturation effects.

IV. NUMERICAL RESULTS AND DISCUSSION

In Fig. 2, we compare predictions of various dipole models with data for inclusive prompt-photon production from RHIC at $\sqrt{s} = 200$ GeV and from the Tevatron at $\sqrt{s} = 1.8$ TeV. A word of caution is in order here. All the above parametrizations for the dipole cross-section have been fitted to DIS data at $x \leq 0.01$. This corresponds to $p_T \leq 2$ GeV at the RHIC energy, so the PHENIX data plotted in the upper panel of Fig. 2 are not suited for a model test. Notice that the CDF data plotted in the bottom panel of Fig. 2 were obtained with a so called isolation cut, which is aimed at suppression of the overwhelming background of secondary photons originated from radiative hadron decays. This might change the cross-section within 10 – 20% for the CDF kinematics [30].

One can see from Fig. 2 that various dipole models presented in the previous section with explicit saturation give rather similar results at small p_T . At high p_T , CGC, b-CGC and GBW-DGLAP models which incorporate QCD evolution provides a better description of data compared to the GBW model. It is clear that the dipole model without explicit saturation as given by Eq. (15) with $\gamma_s = 0.43$, does not describe the data either from PHENIX, or from CDF (we do not show in Fig. 2, No Sat. with $\gamma_s = 0.43$ curve for CDF, since it is about two orders of magnitude above the other models and data). However, changing the anomalous dimension to the DGLAP value with $\gamma_s = 1$, dramatically changes the results and brings the curves (No Sat model) at both energies of RHIC and Tevatron (at $\eta = 0$) within the ranges of other dipole models with saturation. As we commented above, such a behavior of anomalous dimensions allows to conclude that this experiment should be sensitive to the saturation effects.

We have recently shown that the color dipole formulation coupled to the DGLAP evolution provides a better description of data at large transverse momentum compared to the GBW dipole model [4]. In Fig. 3, upper panel, we show the predictions of the GBW (with charm quark) and the GBW-DGLAP models for LHC energies $\sqrt{s} = 5.5, 14$ GeV at midrapidity for the transverse momentum up to $p_T = 200$ GeV. In Fig. 3, lower panel, we show the predictions of various color-dipole models for $\sqrt{s} = 14$ GeV at different rapidities. Generally, the

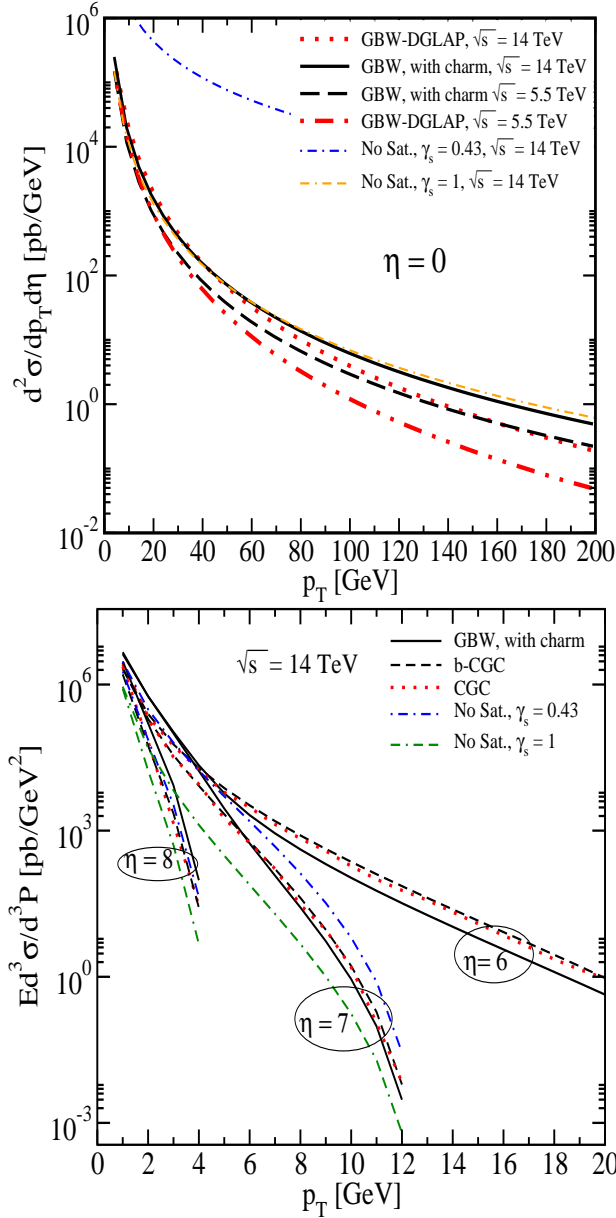


FIG. 3: Direct photon spectra obtained from various dipole model at midrapidity (upper panel) and forward rapidities (lower panel) at the LHC energies for pp collisions.

discrepancy among predictions of various models at moderate p_T is not very large. This can be also seen from Fig. 4 where we compare, as an example, the GBW and b-CGC models, which expose very different structures (see Eqs. (7,13) and Fig. (1)). In the inserted plot in Fig. 3, we show the effect of unitarization within the GBW model, namely using the exponent in Eq. (7) as a dipole cross-section (r_2 model). One can also see that the discrepancy between the GBW and the r_2 model increases at forward rapidities, though it is still not appreciable.

In Fig. 3, we also show the results for the model without saturation. At the midrapidity again the predictions of the No Sat

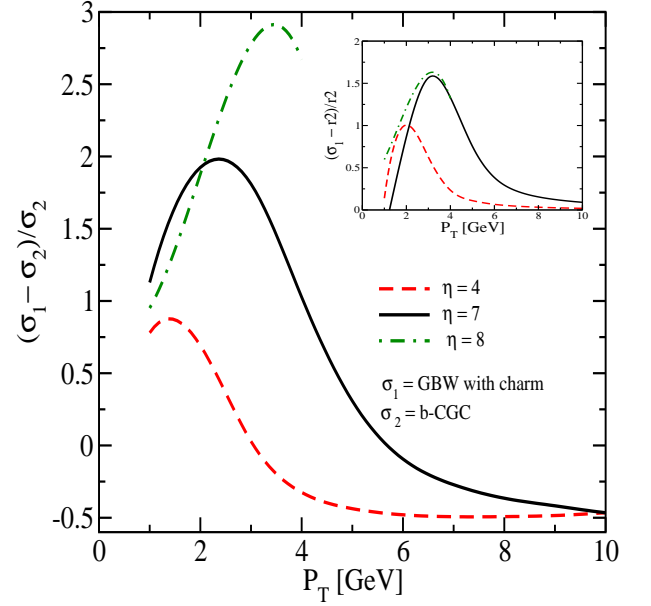


FIG. 4: The difference between the GBW and the b-CGC models for the LHC energy $\sqrt{s} = 14$ TeV at different rapidities. Inserted plot: the discrepancy between the GBW and the r_2 model (the GBW model without explicit saturation) at various rapidities for $\sqrt{s} = 14$ TeV in pp collisions.

model with the DGLAP anomalous dimension $1 - \gamma_s = 0$ is close to other saturated models. At the same time, at very forward rapidities, the anomalous dimension $1 - \gamma_s = 0.57$ which is close to the value predicted from the BK equation [24], will be in favour of other saturated models. This indicates that direct photons production at different rapidities at LHC is rather sensitive to the saturation, and can be used as a tool to measure the anomalous dimension. Again, since the values of anomalous dimension turn out to be larger than $\gamma_{cr} = 0.37$, such a description of the experimental data indicates at a large saturation effect.

In Fig. 5, the differential cross-section of photon radiation at the energy of LHC is plotted versus rapidity at fixed transverse momenta $p_T = 1, 3, 5$ GeV. Calculations were performed with several models for the dipole cross section. All of them lead to a substantial enhancement of the photon production rate at forward rapidities. One can see that the larger the saturation scale is, the stronger is the peak. From Fig. 5, it is again obvious that No Sat model at very forward rapidity is within the dipole model's predictions with an explicit saturation. However, the peak disappeared since at about midrapidity $\gamma_s = 0.43$ is too small. In principle, the peak can be also reproduced in the No Sat model if one allows an anomalous dimension running with energy and transverse momentum p_T . The appearance of the peak at forward rapidity is a direct consequence of the abelian nature of the electromagnetic interaction. In the case of gluon radiation, the peaks at forward-backward rapidities is replaced with a kind of plateau at central rapidities, which is indeed observed in data for hadron production.

To conclude, by this letter we encourage measurements of

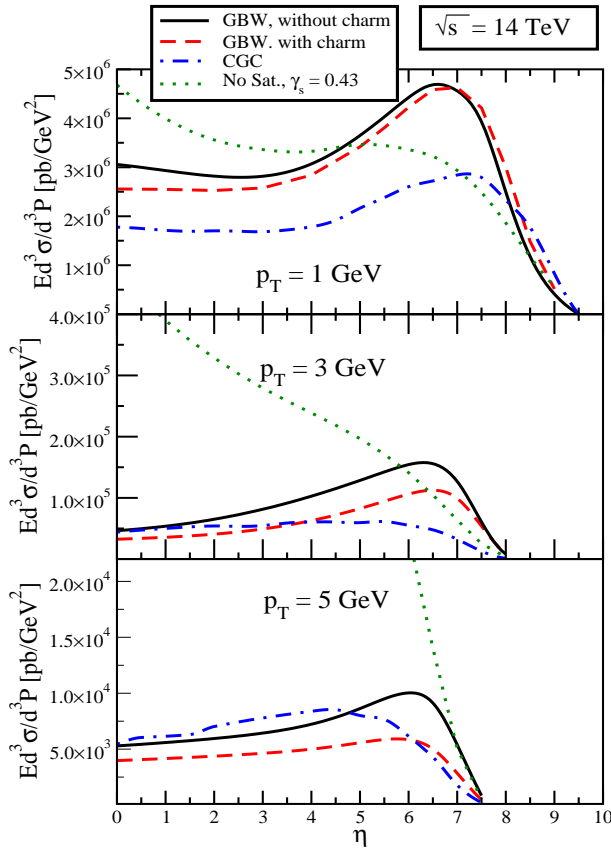


FIG. 5: Invariant cross-section for direct photon production in pp collisions as a function of rapidity calculated with various color dipole models η for various fixed p_T shown in the plots.

direct photons at forward rapidities in pp collisions at modern colliders. These experiments will be a sensitive tool for search for saturation effects, since they will allow to access the smallest possible values of Bjorken x in the target. Besides, the background of photons from radiative hadronic decays should be significantly suppressed. As we demonstrate in Fig. 5, direct photons are enhanced, even form a bump, at forward rapidities. At the same time, gluon nonabelian radiation is known to be strongly suppressed in this region, so hadron and decay photons are also suppressed. We provided predictions for the cross section of direct photon production at various rapidities for pp collisions at LHC employing different models for the dipole-proton total cross section.

Acknowledgments

This work was supported in part by Conicyt (Chile) Programa Bicentenario PSD-91-2006, by Fondecyt (Chile) grants 1070517, 1050589 and by DFG (Germany) grant PI182/3-1, by BSF grant # 20004019, by a grant from Israel Ministry of Science, Culture & Sport, and the Foundation for Basic Research of the Russian Federation.

-
- [1] B.Z. Kopeliovich, Soft Component of Hard Reactions and Nuclear Shadowing (DIS, Drell-Yan reaction, heavy quark production), in proc. of the Workshop Hirschegg'95: Dynamical Properties of Hadrons in Nuclear Matter, Hirschegg, January 16-21, 1995, ed. by H. Feldmeier and W. Nörenberg, Darmstadt, 1995, p. 102 (hep-ph/9609385).
 - [2] B.Z. Kopeliovich, A. Schäfer and A. V. Tarasov, Phys. Rev. **C59** (1999) 1609.
 - [3] B. Z. Kopeliovich, E. M. Levin and I. Schmidt, work in progress.
 - [4] B. Z. Kopeliovich, A. H. Rezaeian, H. J. Pirner and I. Schmidt, Phys. Lett. **B653**, 210 (2007)[arXiv:0704.0642].
 - [5] A. H. Rezaeian, B. Z. Kopeliovich, H. J. Pirner and I. Schmidt, arXiv:0707.2040.
 - [6] B. Z. Kopeliovich, H. J. Pirner, A. H. Rezaeian and I. Schmidt, Phys. Rev. **D77**, 034011 (2008)[arXiv:0711.3010]; B. Z. Kopeliovich, A. H. Rezaeian and I. Schmidt, Nucl. Phys. **A807**, 61 (2008)[arXiv:0712.2829]; B. Z. Kopeliovich, A. H. Rezaeian and I. Schmidt, arXiv:0804.2283.
 - [7] N. Armesto *et al.*, J. Phys. **G35**, 054001 (2008) [arXiv:0711.0974].
 - [8] R. E. Blair, S. Chekanov, G. Heinrich, A. Lipatov, and N. Zotov, Proceedings of the HERA-LHC workshop (CERN-DESY), 2007-2008, arXiv:0809.0846.
 - [9] L. V. Gribov, E. M. Levin and M. G. Ryskin, Phys. Rept. **100**, 1 (1983).
 - [10] L. McLerran and R. Venugopalan, Phys. Rev. **D49**, 2233 (1994); **D49**, 3352 (1994).
 - [11] I. Arsene *et al.* [BRAHMS Collaboration], Phys. Rev. Lett. **93**, 242303 (2004) [arXiv:nucl-ex/0403005].
 - [12] B. Z. Kopeliovich, J. Nemchik, I. K. Potashnikova, M. B. Johnson and I. Schmidt, Phys. Rev. **C72**, 054606 (2005) [arXiv:hep-ph/0501260].
 - [13] J. F. Gunion and G. Bertsch, Phys. Rev. **D25**, 746 (1982).
 - [14] B. Z. Kopeliovich, J. Raufeisen and A. V. Tarasov, Phys. Lett. **B503**, 91 (2001) [arXiv:hep-ph/0012035].
 - [15] B. Z. Kopeliovich, A. H. Rezaeian, arXiv:0811.2024.
 - [16] S. J. Brodsky, A. S. Goldhaber, B. Z. Kopeliovich and I. Schmidt, Nucl. Phys. **B807**, 334 (2009) [arXiv:0707.4658].
 - [17] SMC Collaboration, Phys. Rev. **D58**, 112001 (1998).
 - [18] K. Golec-Biernat and M. Wüsthoff, Phys. Rev. **D59**, 014017 (1999); **D60**, 114023 (1999).
 - [19] H. Kowalski, L. Motyka and G. Watt, Phys. Rev. **D74**, 074016 (2006).
 - [20] J. Bartels, K. Golec-Biernat and H. Kowalski, Phys. Rev. **D66**, 014001 (2002).
 - [21] E. Iancu, K. Itakura and S. Munier, Phys. Lett. **B590**, 199 (2004).
 - [22] E. Levin and K. Tuchin, Nucl. Phys. **B573**, 833 (2000)[arXiv:hep-ph/9908317].

- [23] G. Watt and H. Kowalski, Phys. Rev. **D78**, 014016 (2008).
- [24] D. Boer, A. Utermann and E. Wessels, Phys. Rev. **D75**, 094022 (2007)[arXiv:hep-ph/0701219].
- [25] B. Z. Kopeliovich, I. K. Potashnikova and I. Schmidt, Phys. Rev. **C73**, 034901 (2006) [arXiv:hep-ph/0508277].
- [26] J. Bartels and E. Levin, Nucl. Phys. **B387**, 617 (1992); A. H. Mueller and D. N. Triantafyllopoulos, Nucl. Phys. **B640**, 331 (2002)[arXiv:hep-ph/0205167]; S. Munier and R. B. Peschanski, Phys. Rev. **D69**, 034008 (2004)[arXiv:hep-ph/0310357]; Phys. Rev. Lett. **91**, 232001 (2003)[arXiv:hep-ph/0309177].
- [27] M. Gluck, L. E. Gordon, E. Reya and W. Vogelsang, Phys. Rev. Lett. **73**, 388 (1994).
- [28] CDF Collaboration, Phys. Rev. **D70**, 074008 (2004).
- [29] PHENIX Collaboration, Phys. Rev. Lett. **98**, 012002 (2007).
- [30] CDF Collaboration, Phys. Rev. Lett. **73**, 2662 (1994); **74**, 1891 (1995).